ESTIMATION OF FATIGUE RESIDUAL LIFE OF THE SUPERIOR I-BEAM OF AN OILFIELD PUMPING UNIT

Larrainzar César, clarrain@uncoma.edu.ar
GMF - UNCOMA / ANPCyT. Buenos Aires 1400. (8300) Neuquén. Argentina

Perez Ipiña Juan, pipina@uncoma.edu.ar
GMF - UNCOMA / CONICET. Buenos Aires 1400. (8300) Neuquén. Argentina

Abstract. *A study of the fatigue residual life of the superior I-beam of an oilfield pumping unit is presented. The I-beam was broken after ten years of operation, because of the propagation of a crack by fatigue.*

Lifting lugs had been welded on the upper flange of the I-beam at the moment of assembling the machine. Probably, the weld joint gave place to the crack nucleation, that grew by fatigue up to the critical condition that produced the instability of the I-beam, leaving out of operation the machine with the consequent economical loss for the operating company.

As the company owns several other units operating in similar conditions, the estimation of fatigue residual life presents interest in order to plan the inspection periods of non destructive tests (NDT), so that, any crack which is growing by fatigue can be detected, and repaired, before reaching its critical size and then avoiding the catastrophic failure of the component.

To analyse the fatigue crack growth process, the design and operating characteristics of the unit and its dimensions were obtained. The stress cycle in the failure zone was estimated, the mechanical properties of the steel used in the I-beam were determined, the final failure conditions were analysed by using the Failure Assessment Diagram (FAD) and the fatigue residual life was then estimated using the Paris-Erdogan Law. Later, different operation situations were covered.

Finally, based on the results obtained, an interval of 24 months between consecutive inspections to the NDT was proposed.

Keywords*: residual life, pumping unit, Failure Assessment Diagram, fatigue crack growth.*

1. INTRODUCTION

A pumping unit is designed to extract oil from the well: an electric motor (or combustion engine) gives the necessary power to the reciprocant movement of the crank-handle mechanism, the movement is transmitted to I-beam (also called walking beam) and then to the wireline in order to pump the oil from the depth. Several pumping units are usually installed in the same reservoir, working many times at different operating conditions.

These machines are operated for long periods and they have a schedule for programmed maintenance stops, nevertheless, they are also visited, in shorter periods, for visual inspections and verification of their good operation conditions.

The study of fatigue residual life of the superior I-beam of an oilfield pumping unit is shown in the present work. The I-beam was broken after ten years of operation, the failure occurred because of fatigue crack propagation, this failure took place suddenly, after a visual inspection had been carried out.

From the information provided by personnel of the company, at the moment of assembling the machine, lifting lugs were welded in the superior flange of the I-beam by manual arc welding process with no qualified weld procedure nor post weld heat treatment. This situation occurred around the second half of the 90`s decade. Then, the machine was operating for around 120 months, until its superior I-beam broke catastrophically, generating a complicated situation at the moment of repairing the machine. The company that required this study was concerned with this problem since two failures had already occurred, while several identical pumping units are operating in similar operating conditions.

The objective of this work was to provide a tool that allows the company to program the inspection periods and, in this way, to avoid more failures of this type, that leave out of operation the machine with the consequent economical loss.

2. MATERIAL AND METHOD

The following steps were carried out in this study:

- All the dimensions and characteristics of the unit were obtained (according to the manufacturer`s technical specifications).

- The load cycle in the wireline of the pumping for a given operating condition was obtained from the surface card.
- The kinematic chain of the machine was analyzed in order to estimate the loads on the superior I-beam.
- The stress cycle at the failure zone was determinated.
- The mechanical properties and the type of steel were got by means of:
  - Chemical composition.
  - Tension tests.
  - Fracture toughness tests (CTOD) at different temperatures.
- The fracture surface of the I-beam was macroscopically analyzed.
- The conditions at the final instability were analyzed with the aid of the Failure Assessment Diagram (FAD) of API 579.
- The estimation of the fatigue residual life was performed.
- Different situations were covered and, based on these results, the inspection´s period for Non Destructive Testing (NDT) were suggested.

2.1 Characteristics of the pumping unit

Figure 1 is a schematic representation of a similar pumping unit to the failed unit. The failure zone and the nomenclature of different parts are also indicated in this figure.

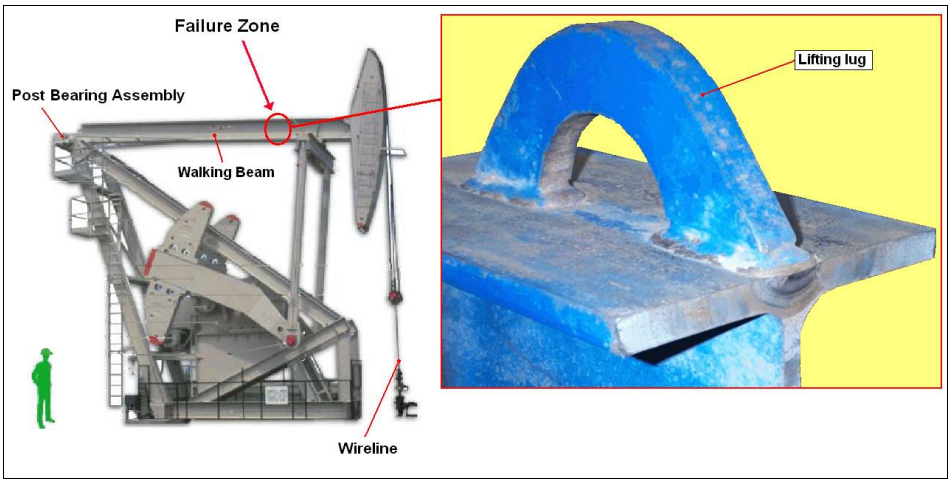

Figure 1. Schematic representation of the pumping unit with a detail of the failure zone.

The data corresponding to the loads measured in the wireline of pumping, for a given operating condition, supplied by the operator, are shown in Fig. 2. The loads acting on the element in study were calculated from these data.

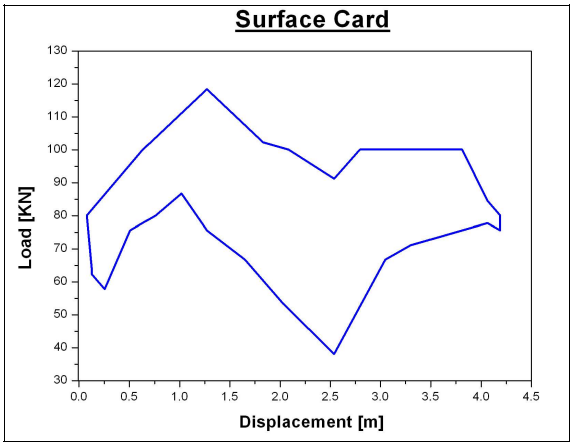

Figure 2. Surface card to an operating condition.

3. RESULTS

3.1 Stress cycle at the failure zone

The kinematic chain of the pumping unit, considered as a four bars mechanism, was solved and then, with the information of the surface card, the I-beam dimensions and the geometric characteristics of the profile of Fig. 3, the bending, shear and tension diagrams were obtained. Then, the stress cycle at the failure zone was estimated, having

resulted of an amplitude as given by Eq. (1). Figure 4 shows the simplified stress cycle on the failure zone that was considered in this part of the analysis.

$$\Delta\sigma = 38\ MPa \tag{1}$$

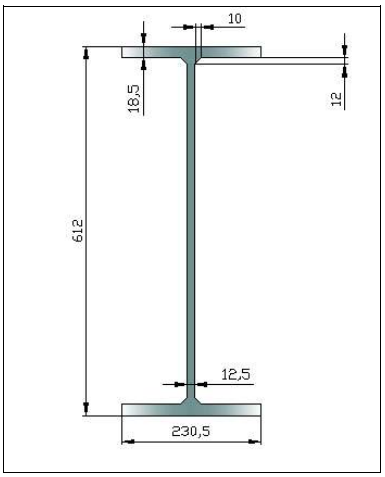

Figure 3. Geometry of the profile.

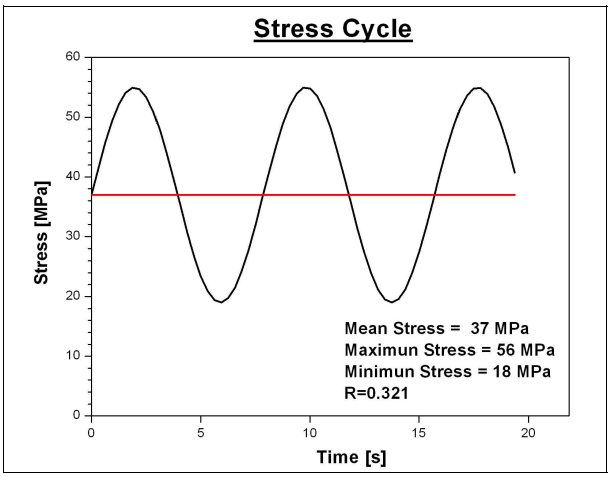

Figure 4. Cycle of stress.

3.2 Characterization of the steel

As there was not available information of the type of steel used in the I-beam, a spark spectrometer was used in order to determine the chemical composition. It is shown in Tab. 1.

Table 1. Chemical composition of the steel (wt %).

	C	Si	Mn	Cr	Mo	Ni	Al	Co	Cu
	%	%	%	%	%	%	%	%	%
x̄	0.100	0.278	1.12	0.071	0.018	0.110	0.018	0.016	0.278
s	0.006	0.012	0.017	0.002	0.003	0.004	0.008	0.005	0.009
sr	5.844	4.363	1.479	3.466	16.594	3.369	40.840	32.362	3.324

	Nb	Ti	V	W	Pb	Zr	Fe
	%	%	%	%	%	%	%
x̄	<0.005	<0.001	0.027	0.045	0.039	<0.003	97.9
s	0.002	0.001	0.001	0.022	0.011	0.001	0.053
sr	42.480	116.230	4.555	48.768	26.756	27.126	0.054

According to the chemical composition, it could be an ASTM A131 / A131 M-04 Grade AH32 steel and, according to designation of UNS, an UNS - K 11846 steel.

To characterize the mechanical properties of the steel, tension and fracture toughness tests at different temperatures were also performed. Table 2 shows the tension test results at room temperature (25ºC) performed according to ASTM E 08 (2001), corresponding to two specimens extracted from the failed I-beam.

Table 2. Tension test at room temperature, 25ºC.

σ_{ys} [MPa]	σ_u [MPa]	Elongation [%] l_0 = 50 mm
383	490	40
392	488	41

CTOD tests according to ASTM E 1820 (2005) were performed to characterize the fracture toughness at different temperatures. The specimens were the single edge three point bending type, SE(B), with thickness-to-height ratio, **B/W = 0.5**, and they were extracted from the failed I-beam in L-T direction of the profile according to ASTM E 1823 (2002). Figure 5 shows the obtained Load (P) versus Crack Mouth Opening Displacement (CMOD) records and Tab. 3 shows the results for the maximum load CTOD.

Table 3. Results of the fracture toughness tests, CTOD.

Specimen	I	II	III
T [ºC]	-15	-15	27
$CTOD_{Pmax}$ [mm]	0.82	0.83	0.71

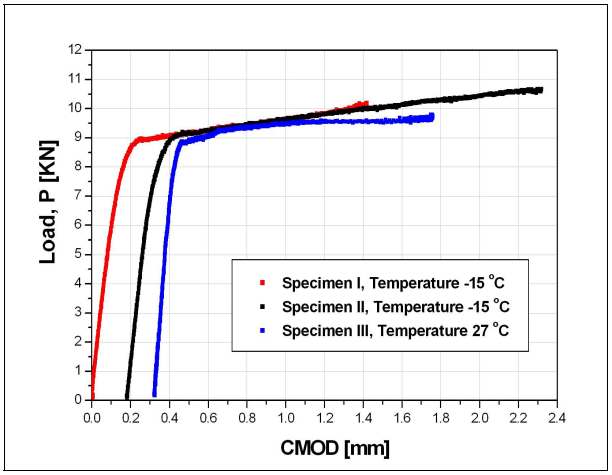

Figure 5. Load versus CMOD records for CTOD tests.

3.3 Analysis of the Crack Propagation

The fracture surface is shown in Fig. 6, where it can be seen that, at the beginning, a single crack front was growing by fatigue; when the crack front arrived to the web, an unstable crack growth and arrest happened (called ductile instability in the figure) and then the crack continued growing by fatigue although with three fronts. To analyze the fatigue crack advance, the crack growth was divided in two stretches, just to make the analysis simpler. The first stretch ranged from a small crack size, up to beginning of the ductile instability. The second stretch started at the arrested crack front in the web and the corresponding fronts in the flange, up to the final instability. The crack propagation for both stretches was supposed driven only by fatigue.

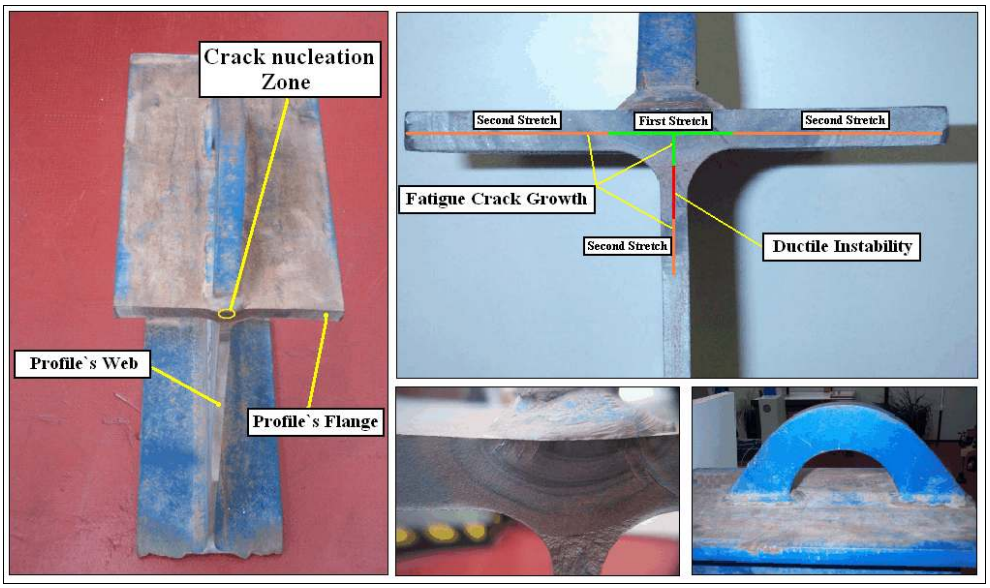

Figure 6. Photos of the I-beam that failed where beach marks can be observed.

The terminology used to characterize dimensionally the crack geometry is shown in Fig. 7, where **2*a*** is the major length of the crack; **c** is the minor length or depth through flange`s thickness; and ϕ is the angle corresponding to the point on a circumference with radio **c**.

First Stretch

Some beach marks corresponding to the first stretch analyzed are shown schematically in Fig. 7. The beach marks used in this work have been enumerated on the fracture surface in upward order in the direction of crack advance.

"Mark 1" corresponds to the first beach mark that could be clearly determined by macroscopic examination on the crack front, and **"Mark 4"** corresponds to the final beach mark for the first stretch of the analysis.

The stress intensity factor amplitudes, **ΔK**, at different points of this crack fronts were calculated in the flange`s direction (ϕ = 0º) and web`s direction (ϕ = 90º). This analysis was repeated for the different crack fronts corresponding to beach marks relieved and enumerated from fracture surface,**"Mark 1"**,**"Mark 2"** and **"Mark 3"**, nevertheless to **"Mark 4"** was not possible.

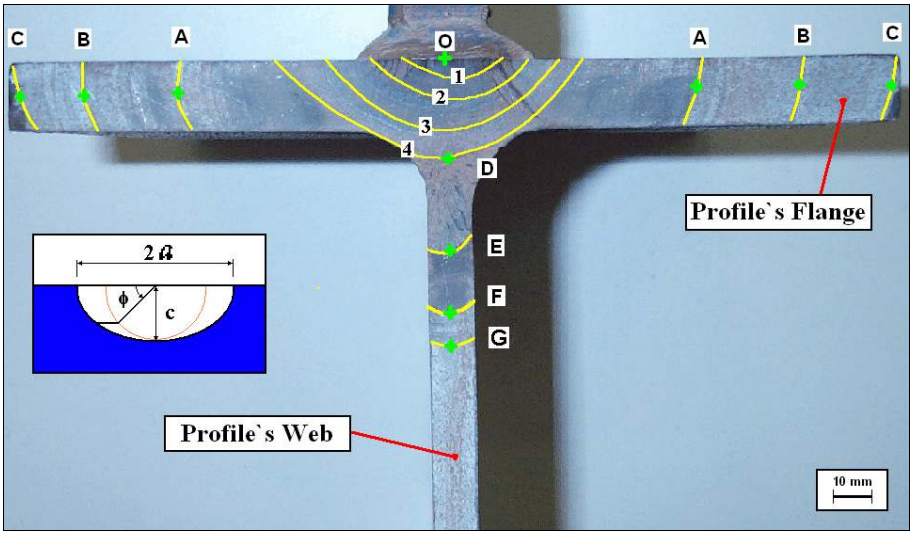

Figure 7. Fracture surface with beach marks and crack geometry nomenclature.

The crack model for the stress intensity factor calculation in the first stretch was the semi-elliptical crack in finite plate under tension (Murakami Y., 1987).

Second Stretch

The considered second stretch in the analysis of the crack growth can be observed in Fig. 7, this stretch includes the advance from **"Mark 4"** up to the final fracture of the I-beam, points **C** (in the flange) and **G** (in the web).

Once the crack front was at **"Mark 4"**, and due to the fact that under these conditions the flange and the web were separated, an unstable condition at the crack tip corresponding to profile`s web was reached, given place to a fast crack growth of about 24 mm (from point **"D"** up to point **"E"**). At point **"E"**, and very probably as consequence of a stress redistribution, the crack was arrested.

After the instability, the crack advanced again by fatigue, with three fronts, two of these by the flange with opposite senses (from **"Mark 4"** up to **"C"**) and the remaining one by the web from **"E"** until **"G"**.

Once again, for the crack growth analysis in this second stretch, the different values that the stress intensity factor range had at the crack fronts were calculated. Using these values the crack growth rates were calculated.

The models of cracks for the stress intensity factor calculation in the second stretch were different for the web than for the flanges. The finite plate with a crack of length ***c*** (it to said with a tip) under pure bending was considered for the web, and the finite plate with a center crack of length ***2a*** (it to said with two tip) under tension was used for the flange direction, (Murakami Y., 1987).

3.4 Analysis of instability by means of the FAD

The conditions for the final instability were analyzed using the **F**ailure **A**ssessment **D**iagram (**FAD**). Originally, the **FAD** considered the linear elastic fracture mechanics (LEFM) and the plastic collapse, as two extreme forms of failure of the cracked component (Perez Ipiña, J., 2004). Nowadays, the newer versions also contemplate the elastic-plastic fracture mechanics, however, for the present analysis a simple option was used.

For the present analysis two parameters were evaluated, the first one, $\mathbf{K_r}$, given by Eq. (2).

$$K_r = \frac{K_I(a,\sigma)}{K_{IC}} \qquad (2)$$

where $\mathbf{K}_I$ is the applied stress intensity factor and $\mathbf{K}_{IC}$ is the fracture toughness of the material. And the second one is given by Eq. (3),

$$S_r = \frac{\sigma}{\sigma_L} \tag{3}$$

Equation (3) gives the relationship among applied stress, **σ**, on the remaining ligament and the plastic collapse stress, $\boldsymbol{\sigma}_L$. For the case in study, the material yield stress ($\boldsymbol{\sigma}_{ys}$) was considered as the plastic collapse stress.

The estimations of the applied stress, **σ**, on the remaining ligament were made for different crack sizes of the fracture surface shown in Fig. 7. Once generated the crack, it began to propagate by fatigue, normally to the axial axis of the I-beam. As the crack advanced, the resisting area of the profile decreased and also its moment of inertia, generating an increment of the stress in the remaining ligament that still had the profile.

The **FAD**, taken from API Recommended Practice 579 - section 9 (2000), defines acceptable and unacceptable regions of a flawed component, by the following equation,

$$K_r = \left(1 - S_r^{2.5}\right)^{0.20} \tag{4}$$

To use the **FAD**, the material fracture toughness is required, this value was estimated from the CTOD tests by mean of Eq. (5).

$$K = \sqrt{n E \sigma_{ys} \delta} \tag{5}$$

Where **δ** is the CTOD value, in the present work the CTOD to maximum load was considered, **E** is the elastic modulus of the material (210 GPa), $\boldsymbol{\sigma}_{ys}$ is the yield stress and **n** is a parameter that can take different values between 1 and 3 (Perez Ipiña, J., 2004). The calculated values of $\mathbf{K}_{IC}$, for **n** = 2, are shown in Tab. 4.

Table 4. Estimation of $\mathbf{K}_{IC}$.

T [°C]	**-15**	**-15**	**27**
$\mathbf{K}_{IC}$ [MPa $\mathbf{m}^{1/2}$]	**365**	**367**	**340**

Figure 8 shows Eq. (4) and the points corresponding to the values of $\mathbf{K}_r$ and $\mathbf{S}_r$ for the different crack sizes measured at the fracture surface, the last point corresponding to **G** in Fig. 7.

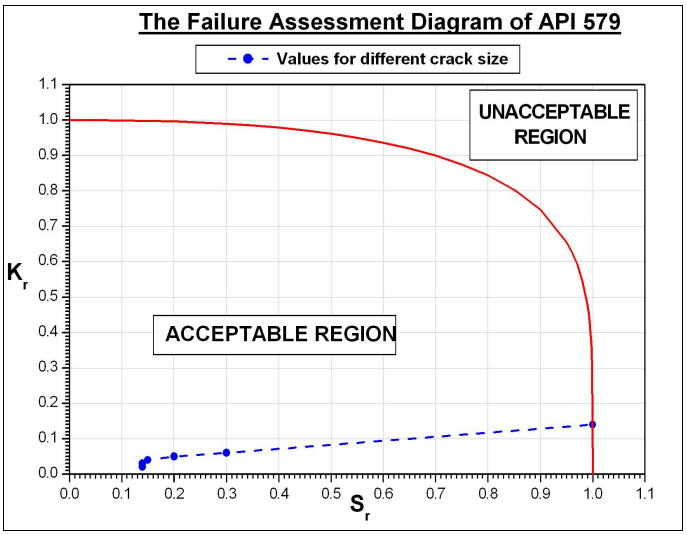

Figure 8. The Failure Assessment Diagram of API 579.

3.5 Estimation of the Fatigue Residual Life

The fatigue crack growth can be described by using the Paris-Erdogan Law (Anderson T. L., 1995). For the case of the ferritic-pearlitic steel at room temperature in air or in other non-aggressive environments, according to API Recommended Practice 579 - Appendix F (2000), this law is written as:

$$\frac{da}{dN} = C\Delta K^m = 6.89 \times 10^{-9}\ \Delta K^3 \qquad \left(\frac{mm}{cycle};\ MPa\sqrt{m}\right) \tag{6}$$

This equation expresses the crack propagation rate, **d*a*/dN**, as a function of the variation of the applied stress intensity factor, being **C** and **m** constants in Paris-Erdogan Law.

The number of cycles of crack propagation up to the structural collapse may be expressed as (Barson J. M. et al 1999):

$$N = \int_{a_i}^{a_f} \frac{1}{C\,(\pi a)^{\frac{m}{2}}\ \Delta\sigma^m\, Y^m}\, da \tag{7}$$

where, **N** : cycles spent in the advance of the crack from a_i to a_f, a_i = initial crack size, a_f = final or critical crack size, and **Y** : geometric factor.

As the analytical resolution of Eq. (7) is too complex, a numerical integration was performed in order to know the total number of cycles consumed up to the failure, as is shown in Eq. (8),

$$N = \sum_{a_i}^{a_f} \frac{\Delta a}{C\,(\pi a)^{\frac{m}{2}}\ \Delta\sigma^m\, Y^m} \tag{8}$$

where: Δa = small finite advance of the crack.

The considered hypothesis to apply the Paris-Erdogan Law were in this case:

- The application of LEFM is valid.
- A sinusoidal stress cycle was supposed.
- Neither overloads nor stops were considered.
- Different-to-sub-critical fatigue crack growth mechanisms were not considered (as example, stress corrosion cracking).
- The fatigue crack propagation threshold (at least in first approximation) was not considered.
- Residual stress fields and stress concentration in the zone of the weld were not considered.
- The fatigue crack initiation life was not considered.

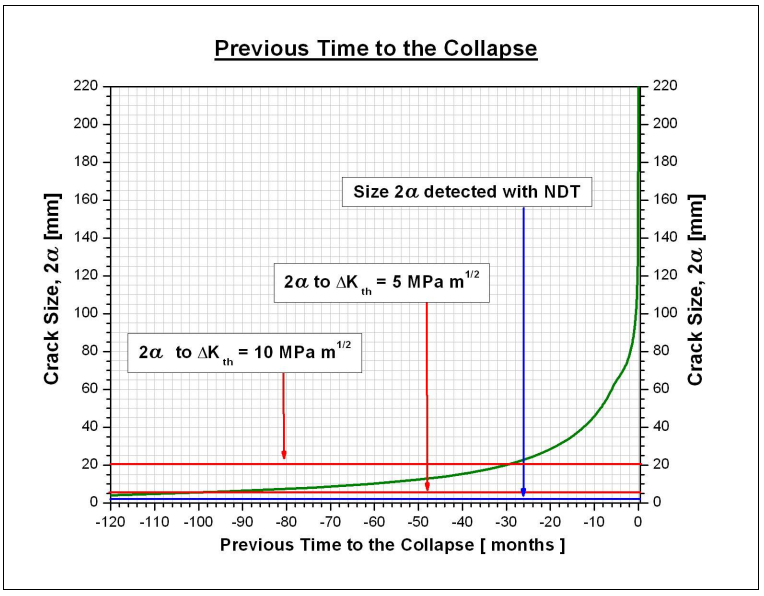

Figure 9. Previous time to the collapse for primary case.

The number of cycles from the "initial" crack size to the crack size that produced the collapse of the structure was calculated. Then, the time consumed was estimated and a graph of the previous months to the component failure as a function of the crack size was build, as it is shown in Fig. 9. This graph also includes:

- The crack size **$2a$ = 5.5 mm**, corresponding to the fatigue threshold ΔK_{th} given by API Recommended Practice 579 (2000), in this case: ΔK_{th} = 5 MPa $m^{1/2}$.
- The crack size **$2a$ = 21 mm**, corresponding to the fatigue threshold ΔK_{th} that present the steel similar to the used in the I-beam, ΔK_{th} = 10 MPa $m^{1/2}$.
- The crack size **$2a$ = 1.5 mm**, corresponding to a crack size that, according to the company, can be detected with a routine NDT.

3.6 Variability Analysis

The case above analyzed is just an ordinary situation in the operating conditions for this type of equipment, although it is not the only situation that can be present during the operation, therefore an analysis of variability was performed.

Reference Case: the stress cycle in the welded zone with an amplitude $\Delta\sigma$ = 38 MPa and a mean stress σ_m = 37 MPa was analyzed. An operating regime of the unit of 0.12 Hz (7.2 strokes per minute, SPM) and the Paris-Erdogan constants of Eq. (6) from API 579 were used.

The variations that can occur in the operation of the unit pumping, or in similar units under different conditions of operation, and that were analyzed in this work, are detailed now.

The torque of these pumping units can vary from 62 % to 108 % of the nominal torque (**NT**), that for this machine is **NT** = 72.3 kN m (53.3 kpi-ft). Then, the lower operating torque (**LT**) must be approximately **LT** = 44.8 kN m (33 kpi-ft) and the maximum torque **MT** = 78.1 kN m (57.6 kpi-ft). For the reference case the operating torque (**OT**) was **OT** = 65.5 kN m (48.3 kpi-ft), below the **NT**. Therefore, the torque was considered approximately oscillating between 69 % and 120 % of the **OT**, because the operating point was located in **LT < OT < NT <MT**.

The operating regime can vary from 0.067 Hz to 0.17 Hz (from 4 to 10 SPM), while in the reference case the operating regimen was 0.12 Hz (7.2 SPM).

These variables influence in the following way, the variation in the torque implies a change in the load applied in the wireline of pumping, that produces a variation in the stresses present on the area of the profile where the lifting lug was welded. According to the variations observed between the **OT** and the **MT**, the present stress has an increase of 20 %; and between the **OT** and the **LT**, it has a decrease of 31%. For the assessments of the fatigue residual life, it was supposed that the variation of the stress is given only in the maximum stress. Then, the maximum stress was considered with an increase of 20 % and a decrease of 31 % for the different analyzed situations.

On the other hand, the change in the operating regime of the unit implies a change in the time to consume the cycles of fatigue that was subjected the I-beam.

Other parameters that influence the time of fatigue residual life are the Paris constants, being the values of Eq. (6) for conservative assessments, although in fact these values can vary with a certain margin for different types of ferritic-pearlitic steels. An increase in **C** of 20% and an increase and decrease of 10% in **m** were considered.

Taking into account the above mentioned, the different cases simulated enclosed most of the operating conditions:

	Δσ [MPa]	**C x 10 $^{-9}$**	**m**	**Hz**
Reference Case	38	6.89	3	0.12
Case 1	49	6.89	3	0.12
Case 2	21	6.89	3	0.12
Case 3	38	8.27	3	0.12
Case 4	38	6.89	3.3	0.12
Case 5	38	6.89	2.7	0.12
Case 6	38	6.89	3	0.067
Case 7	38	6.89	3	0.17
Case 8	49	8.27	3.3	0.17

Figure 10 shows the results of crack sizes as function of the previous time to the collapse for the different cases. The reference case and the most unfavorable case are shown in full lines. The most unfavorable case that gave place to the smaller previous time to the collapse was the Case 8.

4. DISCUSSION

With regard to the motives that led to the failure, probably, the weld joint gave place to the crack nucleation, that grew by fatigue up to the critical condition that produced the instability of the I-beam, leaving out of operation the machine. The probable factors that intervened in the events were, in the crack nucleation: stress concentration in the welded joint, presence of initial small defects in the filler metal, modification of the microstructure and residual stress

fields. Once that a crack was nucleated, it grew by fatigue up to the critical condition that produced the instability of the I-beam.

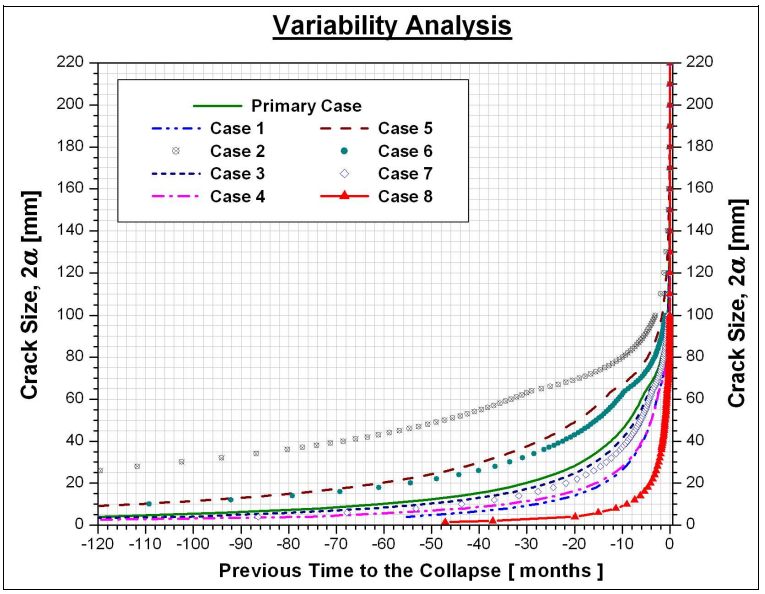

Figure 10. Variability analysis.

For the second stretch analyzed, it was shown that, the fronts that advanced for the flange from the **"Mark 4"** up to point **"A"** had a greater rate, and the front that advanced through the web from point **"E"** up to point **"F"** presented a smaller propagation rate, because **ΔK** in the flange was larger.

When the crack arrived to points **"Mark 4"** at the flange, it grew from point **"D"** to point **"E"** in unstable way and was arrested. Then, it grew once again by fatigue from **Mark 4** to points **A**, **B** and **C** at the flange and from point **"E"** to points **"F"** and **"G"** at the web, as the beach marks in Fig. 7 show. When the crack front attained the points **"C"**, the flange was almost completely cut, occurring the final collapse of the structure.

The **CTOD** tests were carried out at different temperatures (room temperature and -15°C) because, according to the information received from the company, the failures occurred in winter, with minimum temperatures that can attain -15 °C. The possibility of a brittle failure because of the steel was working in the ductile-to-brittle region was considered as possible. **CTOD** results stated that this assumption was wrong: in the whole working temperature range, the steel was working in the upper shelf region.

From the analysis performed on the **FAD**, it can be concluded that the final failure took place by plastic collapse instead of brittle fracture, once the crack crossed the profile`s flange completely, giving place to a great reduction of the inertia moment and the resistant area, with the consequent increase of the actuating stress in the remaining ligament. This result was in concordance with both the observed fracture and the fracture toughness tests results.

The fatigue residual life analysis of Fig. 10 shows that for the reference case, 120 months previous to the collapse, the crack had a size of $2a$ = 4 mm. This crack size is smaller than the size corresponding to the fatigue threshold considered in API 579, however, it could be interpreted that the crack advanced from 4 mm to 5 mm by other sub-critical crack growth mechanism that has not been considered in the present paper, as already mentioned.

Then, the estimation of the crack growth for $\Delta K < \Delta K_{th}$ can be approximated as whether the crack has grown only by fatigue, knowing that an error is introduced. However, this error would not be dangerous, because other possible mechanisms would produce slower crack growth.

As it was described before, a variability analysis was carried out. When the fatigue maximum stress was increased 20% of the reference value, the residual life decreased notably, around 50% . When the operating regime of the unit was increased from 0.12Hz to 0.17Hz, the residual life decreased approximately 30%. For an increment in 20% in the value of constant C in the Paris Law, the residual life decreased around a 10%. Also, an increment of 10% in the value of the coefficient **m** implied a larger rate of crack propagation for the same **ΔK** and therefore a decrement in 35% of the residual life. Finally, the combination of unfavorable variables implied that the fatigue residual life decreased a 60%.

Figure 10 shows that the smallest time for the fatigue residual life of the I-beam from an initial crack size of 1.5mm up to the final fracture is 47 months, corresponds to Case 8, the most unfavorable one. In other words, a pumping unit with the same characteristics and operating under the conditions established for Case 8, with a initial crack of 1.5mm in the weld bead of the lifting lug, assuming that the crack advance is exclusively by fatigue and no threshold exists, will reach the critical size, producing the I-beam collapse, in approximately 47 months. Although this Case 8 corresponds to the most demanding combination for the fatigue residual life, this situation is not very probable. Moreover, this

estimation in the fatigue residual life is conservative because there were considered neither the fatigue initiation cycles, nor the existence of a threshold fatigue crack growth.

4.1 Proposal of NDT periods of inspection

The most important aspect for the company in order to operate the equipment in a reliable way, that is, to have inspection periods that assure that any crack that is growing by fatigue will be detected before it reaches its critical size. Then, the most unfavorable case, Case 8, was selected to estimate the time among inspections.

Accepting the half of the fatigue residual life as the period between **NDT** inspections, they could be carried out every 23.5 months. This value is theoretical, and to contemplate operating situations, the proposed inspection period corresponded to an interval of 24 months. Therefore, there is no possibility, between two consecutive inspections, that a non-detected crack can grow up to the critical sizes and produce the collapse of the structure. The inspections should be carried out with a **NDT** technique that assures a level of detection of 1.5 mm or smaller cracks.

For example, and assuming conditions corresponding to Case 8, if a non-detected crack 1.5 mm long begins to grow the day after a **NDT** inspection. 24 months after that time the crack would be detected approximately with a size of 4 mm, leaving a minimum security margin of 23 months before reaching the critical size.

Another example: suppose that a crack of 2.5 mm at the moment of **NDT** inspection was not detected because of any reason (human error, subsurface crack, or other); at the moment of the next inspection the crack will have a size of 9 mm, and now it will be detected easily. There will remain 10 months before reaching the critical size and attain the conditions to leave the pumping unit out of service.

5. CONCLUSIONS

- The weld joint was the origin of the initiation and propagation of the crack.
- The final failure was by plastic collapse once the crack crossed the profile`s flange completely, as the **FAD** analysis showed.
- The fatigue residual life for an initial crack of 1.5mm varied from more than 120 months to 47 months for the analyzed cases.
- A period of inspection of 24 months was recommended for **NDT** methods that ensure a level of crack detection of 1.5 mm or smaller.
- This inspection period is recommended for pumping units with similar characteristics and with operation conditions contemplated in this work.

6. ACKNOWLEDGEMENTS

To CONICET (National Council for Scientific and Technological Research) and ANPCyT (National Agency of Scientific and Technological Promotion) for their financial support, Mr. Héctor Pérez of Petrolera Entre Lomas S.A. for his collaboration and Mr. Eduardo Benotti of the LPM/GMF for his permanent collaboration.

7. REFERENCES

Anderson T. L., 1995, “Fracture Mechanics, Fundamentals and Applications ”, CRC Press.

API Recommended Practice 579, 2000, “Fitness for Service ”, Seccion 9, Appendix E and Appendix F, first edition.

ASTM E 1820, 2005, “Standard Test Method for Measurement of Fracture Toughness”, Annual Book of ASTM Standards.

ASTM E 1823, 2001, “Standard Terminology Relating to Fatigue and Fracture Testing”, Annual Book of ASTM Standards.

ASTM E 08, 2001, “Standard Test Method for Tension Testing of Metallic Materials”, Annual Book of ASTM Standards.

Barson J. M. & Rolfe S. T., 1999, “Fracture and Fatigue in structures: Applications of Fracture Mechanics ”, ASTM, 3 edition.

Buschiazzo A., Codega D., Cocco R., Perez Ipiña J., 2002, “Análisis de vida residual a la fatiga de un perno unión biela - manivela de equipo de extracción de petróleo”, Congreso CONAMET / SAM 2002.

Lawson L., Chen E., Meshii M., 1999, “Near-Threshold Fatigue: a Review”, International Journal of Fatigue, vol 21, pp 15-34.

Lufkin oilfield products group , 2006, “General Catalog”.

Murakami Y., 1987, “Stress Intensity Factors Handbook ”, Volumen 1 and 2, Pergamon Press, pp. 11-712-714.

Perez Ipiña, J., 2004, “Mecánica de Fractura”, Editorial Alsina, primera edición.

8. RESPONSIBILITY NOTICE

The authors are the only responsible for the printed material included in this paper.